The Collapse of Rotating Massive Stars in 3-dimensions

Chris L. Fryer and Michael S. Warren
Theoretical Astrophysics, Los Alamos National Laboratory, Los Alamos, NM 87545

ABSTRACT

Most simulations of the core-collapse of massive stars have focused on the collapse of spherically symmetric objects. If these stars are rotating, this symmetry is broken, opening up a number of effects that are just now being studied. The list of proposed effects span a range of extremes: from fragmentation of the collapsed iron core to modifications of the convective instabilities above the core; from the generation of strong magnetic fields which then drive the supernova explosion to the late-time formation of magnetic fields to produce magnetars after the launch of the supernova explosion. The list of observational effects of rotation ranges from modifications in the gamma-ray line spectra, nucleosynthetic yields and shape of supernova remnants caused by rotation-induced asymmetric explosions to strong pulsar radiation, the emission of gravitational waves, and altered r-process nucleosynthetic yields caused by fast-spinning rotating stars.

In this paper, we present the results of 3-dimensional collapse simulations of rotating stars for a range of stellar progenitors. We find that for the fastest spinning stars, rotation does indeed modify the convection above the proto-neutron star, but it is not fast enough to cause core fragmentation. Similarly, although strong magnetic fields can be produced once the proto-neutron star cools and contracts, the proto-neutron star is not spinning fast enough to generate strong magnetic fields quickly after collapse and it is unlikely that magnetic fields will dominate the supernova explosion mechanism. Even so, the resulting pulsars for our fastest rotating models may emit enough energy to dominate the total explosion energy of the supernova. However, more recent stellar models predict rotation rates that are much too slow to affect the explosion, but these models are not sophisticated enough to determine whether determine whether the most recent, or past, stellar rotation rates are most likely. Thus, we must rely upon observational constraints to determine the true rotation rates of stellar cores just before collapse. We end with a discussion of the possible constraints on stellar rotation which we can derive from core-collapse supernovae.

Subject headings: stars: evolution - supernova: general

1. Introduction

The collapse of a massive star to a proto-neutron star releases an enormous amount ($\sim 10^{53}$ ergs) of gravitational energy. This energy is primarily converted into thermal energy and later radiated away in the form of neutrinos. However, if the star is rotating, a sizable amount of the energy released can be converted into rotational energy. LeBlanc & Wilson (1970) proposed that magnetic fields could extract this rotational energy and produce a strong supernova explosion, but when Müller & Hillebrandt (1981) found that large magnetic fields were required for such a mechanism to work, interest in this mechanism declined.

Rotation has still been studied in core collapse, both as a means to produce gravitational waves (see Dimmelmeier, Font, & Müller 2002; Fryer, Holz, & Hughes 2002; New 2003 and references therein) and as a means to produce asymmetric explosions (see Fryer & Heger 2000 - hereafter FH - and references therein). FH found that, at least in 2-dimensional models, rotation weakened the

convection in the rotating plane, ultimately leading to explosions that are strongest along the rotation axis. However, the symmetry axis of these 2-dimensional simulations lay along the rotation axis, and it is difficult to distinguish numerical boundary effects from the true asymmetry in the explosion. The first goal of this paper is to test the conclusions of FH by running a series of 3-dimensional, fully 4π (no boundaries), models of the collapse of rotating stars.

However, rotation may play a larger role in producing explosions for some systems. With the discovery of gamma-ray bursts and hypernovae, rotation has once again been invoked as a source of explosion energy (Woosley 1993; Höflich et al 1996; Iwamoto et al. 1998). In the case of the collapsar GRB model and hypernovae, it is believed that the explosion is driven after the the core has collapsed to a black hole and the explosion engine can take advantage of the enormous rotational energy held by the rapidly rotating outer layers of the star. But some authors (e.g. Akiyama et al. 2003) believe magnetic field generation is efficient enough for rotation to drive an explosion quickly and leave behind a neutron star. We will test this possibility with currently available stellar models.

The level of asymmetry in the explosions not only tests the nature of the collapse model, but also the progenitor itself. Unfortunately, the rotation rate of a star prior to collapse depends sensitively on the recipes used to model angular momentum transport in 1-dimensional stellar evolution codes. On the other hand, interpretations of supernova observations have not yet arrived at a consensus on the level of asymmetry in the explosion: some groups insist large asymmetries are required (Wang et al. 2002 and references therein) while others argue mild asymmetries are sufficient (Nagataki 2000; Hungerford, Fryer & Warren 2003). Better models of the explosion and increased supernova observations will be able to distinguish the level of asymmetry, and hence magnitude of rotation, in the collapse and explosion of massive stars. However, other tests can be, and have been, used to measure the rotation in the core: pulsar spin rates, gravitational radiation, and nuclear yields. We conclude with a discussion of these potential observational tests of core-collapse rotation.

The outline of this paper is as follows: §2 describes our numerical technique and the progenitors used in our simulations, §3 concentrates on the effects of rotation on the standard neutrino-driven supernova mechanism, §4 details the viability of additional effects of rotation on the supernova explosion mechanism beyond the basic neutrino-driven picture: from fragmentation to the magnetic-field supernova mechanism. We conclude with a discussion of the observational signatures from these rotationally-induced modifications to the supernova explosion with an eye towards constraining the rotation of the iron core of a pre-collapse star.

2. Progenitors and Numerical Techniques

For these simulations, we use the 3-dimensional, smooth particle hydrodynamics (SPH) supernova code discussed in Fryer & Warren (2002), Warren et al. (2003). Because these simulations involve rotating progenitors where gravity is less likely to be symmetric, we do not constrain the calculation to spherical gravity, but instead use the tree-based gravity algorithm described in Warren & Salmon (1993,1995), Warren et al. (2003) to calculate the multi-dimensional effects of gravity. In addition, the effects of angular momentum transport through shear forces become more important with our rotating models, and we will concentrate our discussion on the numerical artifacts of this shear.

First, let us discuss our progenitors. To compare with the results of FH, we use the same standard progenitor used by this work: E15B of Heger, Langer & Woosley (2000). To study the effects of different progenitors, we also use model E15A of Heger, Langer & Woosley (2000) and the slowly rotating model 15 $M_\odot$ of Heger, Woosley, & Spruit (2003), corresponding to models SN15A, SN15B, and SN15C respectively in this work (Table 1). Although these models have a range of angular velocities (Fig. 1)[1], they have much lower total angular momenta than what is assumed in most gravitational wave simulations. As a calibration for rotation, we also have run models E15A and E15B with the angular velocity set to zero (models SN15A-nr, SN15B-nr).

We use the angular and radial velocity distri-

[1] FH used only model E15B in their simulations. Note, however, that they erroneously plotted the angular momentum of SN15A in Fig. 3 of their paper.

bution given in Heger et al. (2000) to determine the 3-dimensional velocity vectors onto our initial distribution of particles. Like the Fryer & Warren work, we construct our 3-dimensional star (filling the full 4π star) by setting up a series of radially spaced shells (each filled with randomly, but roughly equally, spaced particles). The separation between shells is set to the mean separation between particles within each shell. This random setup, although it prevents any artifacts based on grid issues, does lead to some density deviations in our initial model. These deviations are largest at composition boundaries (e.g. silicon and oxygen shell boundaries), and do not exceed 10% of the density (in most of the star, the deviation is less than 5%) for a 1 million particle initial model. These variations are on par with the deviations expected from silicon and oxygen flash burning (Bazan & Arnett 1998), so although they are numerical in origin, they may match nature reasonably well.

An important constraint on our models is the numerical shear produced by the artificial viscosity used in most SPH codes (e.g. Benz 1990). This viscosity is generally implemented with the following form:

$$\Pi_{ab} = \begin{cases} \dfrac{-\alpha c_{ij}\mu_{ij} + \beta\mu_{ij}^2}{\rho_{ij}} & \text{if} \mu_{ij} < 0; \\ 0 & \text{otherwise.} \end{cases} \quad (1)$$

Here, $\mu_{ij} = h(\vec{v}_i - \vec{v}_j) \cdot (\vec{r}_i - \vec{r}_j)/(|\vec{r}_i - \vec{r}_j|^2 + \epsilon h^2)$ is the velocity divergence at particle i due to particle j where $\vec{v}_i, \vec{v}_j$ are velocities of particles i, j respectively, $\vec{r}_i, \vec{r}_j$ are velocities of particles i, j respectively, ϵ is a small offset to avoid numerical artifacts from particles very near each other, and h, c_{ij} and ρ_{ij} are the average smoothing length, sound speed and density of particles i and j. α and β are artificial viscosity parameters. Most of our models use this implementation of the artificial viscosity with the standard values for the viscosity terms: $\beta = 2 \times \alpha = 3.0$. However, to test the effects of this viscosity on the angular momentum transport, we have also run one model (SN15A-rv) with these viscous terms reduced by a factor of 10 ($\beta = 2 \times \alpha = 0.3$).

Our collapse simulations model the inner $3\,M_\odot$ of the collapsing star with 1 million SPH particles. The resolution is increased near the entropy-driven convective region, corresponding to an angular resolution of over 20 particles per square degree and a mass resolution better than $10^{-6}\,M_\odot$ per particle. We have run one 5 million particle model using the E15A progenitor (SN15A-hr).

3. Rotational Effects on Collapse and Explosion

For the rotation rates found in modern supernova progenitors, rotation has a limited set of effects on the collapse of a massive star. The primary effects of rotation (see Shimizu, Yamada, & Sato 1994; Kotake et al. 2003; FH and references therein) are: 1) high angular velocity material does not accelerate as much in collapse, leading to weaker bounces and lower entropies for this material, 2) angular momentum limits convection where angular momentum is highest and 3) the deformation in the neutrinosphere causes an asymmetry in the neutrino emission. In this section, we will first concentrate on the purely hydrodynamic effects which FH argued to be the dominate rotation effects. We will then discuss the effects of rotation on the neutrino emission. As we shall show, both effects occur in rotating modles and can contribute to asymmetries in the explosion. The pure hydrodynamic effects occur immediately and are most important for quick explosions ($< 100\,$ms after bounce) which is occurs in our simulations, but neutrino asymmetries will play a larger role if the explosion is more delayed.

3.1. Hydrodynamic Effects of Rotation

In this paper, we will use the term "polar" material for that matter which lies along the axis or pole of the rotation and "equatorial" material for that material which lies in the plane of the rotation. The equatorial material has the bulk of the angular momentum in the collapsing star and it is this material that slows during collapse, resulting in a weaker bounce and lower shock values. It is also in the equator where the angular momentum profile strongly inhibits convection.

The collapse of a massive star occurs when the temperature and density in the iron core become high enough to dissociate the iron (removing thermal pressure) and to induce electron capture (removing electron degeneracy pressure) in the core. The initial compression induces further

electron capture and iron dissociation resulting in a runaway collapse that halts only when the core reaches nuclear densities where nuclear forces cause the core to "bounce". This bounce sends a shock through the star which heats the star, raising its entropy. When the shock stalls (through neutrino and dissociation energy losses), it leaves behind an unstable entropy profile that seeds the convection. This convection is currently believed to be important in the success of the supernova mechanism (Herant et al. 1994; Burrows, Hayes, & Fryxell 1995; Janka & Müller 1996; Fryer 1999; Rampp & Janka 2002). With their 2-dimensional simulations, FH argued that the combined effect of the lower entropy from weaker shocks and the strong angular momentum gradients in the equatorial region of the star led to less convection in this region, and ultimately, weaker explosions along the equator versus the rotation axis. Indeed, FH found that the explosion velocities along the pole were twice as fast as those along the equator. Such asymmetric explosions aid in the outward mixing of the nuclear burning products of the supernova (Nagataki 2000; Hungerford, Fryer, & Warren 2003). In this section, we review the claims of FH to determine whether such strong asymmetries persist in 3-dimensional simulations.

First, let's address the first point from FH: does the polar region reach higher entropies after bounce due to a stronger bounce in the pole? Fig. 2 shows an angular slice of model SN15A-hr just before bounce. The colors show the radial velocity and the vectors denote the direction and magnitude of the velocity. Along the poles, where the centrifugal support is negligible, the velocities are much higher than in the equator. The velocity of the infalling material is approximated by assuming free-fall conditions:

$$v_{\rm infall} \approx \sqrt{\frac{GM_{\rm enclosed}}{r} - \frac{j^2}{r^2}}, \qquad (2)$$

where G is the gravitational constant, $M_{\rm enclosed}$ is the enclosed mass, j is the specific angular momentum of the infalling material, and r is its collapse radius. For the angular momentum in SN15A, the corresponding polar vs. equatorial infall velocities as the $1.2 M_\odot$ shell reaches 75 km are: $6.5, 3.8\times10^9 {\rm cm\,s^{-1}}$ pole vs. equator respectively. When the shell reaches 50 km, the respective infall velocities are: $8\times10^9, 0 (centrifugal hang-up) {\rm cm\,s^{-1}}$ pole vs. equator. The equatorial material simply does not reach the high infall velocity magnitudes that are achieved along the pole. The infalling material stops abruptly when the core "bounces", causing it to shock. The entropy (S) in units of Boltzman's constant per nucleon for such a strong shock (assuming a polytropic equation of state with $\gamma = 4/3$) is:

$$S \approx 9.9 \rho_9^{-1/4} v_{10}^{3/2} {\rm k_B\ per\ nucleon}, \qquad (3)$$

where ρ_9 is the density and v_{10} the velocity of the infalling material in units of $10^9\ {\rm g\,cm^{-3}}, 10^{10}\ {\rm cm\,s^{-1}}$ respectively. The faster moving material along the poles has a stronger shock and its resultant entropy after bounce is greater. Fig. 3 shows the constant entropy isosurfaces for model SN15A-hr 45 ms after bounce. The isosurface for an entropy of $7.5 {\rm k_B}$ per nucleon is slightly elongated along the pole, but exists both in the equatorial and polar regions. By studying increasingly higher entropy isosurfaces (Fig. 3 shows entropy isosurfaces of 7.5, 8.0, and 9.0 $\rm k_B$ per nucleon), we see that the highest entropies are limited to the polar region. We remind the reader that our 3-dimensional simulations model the entire 4π sphere with a randomly distributed shell setup, so these asymmetries can *not* be boundary effects or artifacts of the initial conditions.

The stall of the bounce shock leaves behind a negative entropy gradient which initiates convection above the surface of the proto-neutron star. Due to the higher entropy where the shock velocities were largest, this gradient is much larger along the poles, driving stronger convection in this region. When rotation is included, a negative entropy gradient is not sufficient to drive convection. As FH pointed out, supernova convection is inhibited by the large angular momentum gradient in the poles. For rotating objects where the angular momentum increases with radius, convection occurs only if the negative entropy gradient can overcome the positive angular momentum gradient (also known as the Solberg-Høiland instability criterion - Endal & Sofia 1978):

$$\frac{g}{\rho}\left[\left(\frac{d\rho}{dr}\right)_{\rm adiabat} - \frac{d\rho}{dr}\right] - \frac{1}{r^3}\frac{dj^2}{dr} > 0, \qquad (4)$$

where $g = GM_{\rm enclosed}/r^2$ is the gravitational acceleration with gravitational constant G and

$M_{\rm enclosed}$, ρ, and j, the enclosed mass, density and specific angular momentum respectively at radius r in the collapsed core. Fig. 4 shows the angular momentum part of equation 4 ($1/r^3\, dj^2/dr$) for models SN15B (our fastest rotating progenitor) vs. SN15C (our slowest rotating progenitor) both along the equator and pole. Note that along the equator, this value is 4 orders of magnitude higher for the fast rotating vs. slowly rotating models. Indeed, the constraint is essentially negligible in the poles of both models and even in the equator of the slowly-rotating model. Only models SN15A and SN15B are rotating fast enough that convection is affected by the rotation rate. Fig. 5 shows the upflows (isosurfaces of material moving with outward radial velocities of 3000 km s^{-1}) for many of our models 25 ms after bounce. For our rotating models (SN15A,SN15A-hr,SN15B), the convection is strongest along the poles, but for our non-rotating and slowly rotating models (SN15A-nr,SN15B-nr,SN15C), the convection has no preferred axis. We have thus confirmed the FH claim that convection is strongest in the poles for sufficiently rapidly rotating progenitors. Note, however, the slowly rotating progenitor from Heger et al. (2003) is not rotating fast enough to effect the convection, and hence, the explosion through the neutrino-driven supernova mechanism.

3.2. Neutrino Asymmetries from Rotation

Shimizu et al. (1994) and Kotake et al. (2003) have argued that due to the asymmetry in the neutrinosphere, asymmetric neutrino heating will also drive stronger convection along the poles. Density isosurfaces ($10^{11}, 10^{12}$g cm^{-3}) for model SN15A-hr are shown in Fig. 6. Even the inner 10^{12}g cm^{-3} density isosurface has axis ratios of roughly 1.4:1 equator vs. pole. This asymmetry leads to an asymmetry in the neutrinosphere, and ultimately in the neutrino heating which Shimizu et al. (1994) and Kotake et al. (2003) have argued will drive a jet-like explosion if the explosion mechanism is sufficiently delayed.

In our simulations, however, the shock moves out before such asymmetric heating can make a large difference in the convection, and it is more likely that the asymmetry is entirely due to the purely hydrodynamic effects listed by FH. To determine whether such asymmetric convection yields asymmetric explosions, we must model the propogation of the expanding shock until it develops into an explosion. In 2-dimensions, FH were able to model the explosion 1.5 s past bounce, giving time for the expanding material to develop into an explosion with over 20% of the total explosion energy already converted into kinetic energy. Such long-duration simulations are beyond current computational resources for 3-dimensional simulations. Fig. 7 shows the upflows (isosurfaces of material moving with outward radial velocities of 2000 km s^{-1}) of model SN15A at a series of times past bounce. From Fig. 7, it is clear that as the explosion develops, it remains strongest along the poles and the expanding shock moves out furthest in this direction. It is likely that the resultant explosion will be strongly asymmetric along the poles. Although we can not quantitatively estimate the level of asymmetry from our simulations, given the excellent agreement in the convection with FH, it is not unreasonable to assume that the mean velocity of the ejecta along the poles could be a factor of 2 (or greater) larger than the velocity along the equator in these rapidly rotating explosions (see FH).

4. Other Rotational Effects on the Explosion

As these rotating models collapse, much of the potential energy can be converted into rotational kinetic energy and the rotational energy can exceed the supernova explosion energy. This energy may be tapped to help drive the supernova explosion. If the rotational energy gets high enough, it can cause the core to go unstable and fragment. Strong magnetic fields may also develop quickly and extract the rotational energy to drive the supernova explosion. At late phases, as the core contracts, this rotational energy increases, producing rapidly spinning neutron stars that, if born with strong enough magnetic fields, can be observed as pulsars.

What are the implications for the rotating progenitor stars modeled in this paper? To know this, we must first understand the the evolution of the angular momentum distribution in the collapsing core. As one might expect, most of the angular momentum is concentrated along the equator after collapse in an ellipsoidal core (Fig. 8). Fig. 9 shows the angular momentum in mass zones for

3 separate time slices during the collapse. As the proto-neutron star contracts, the angular momentum is gradually transported out of the central core. For SPH, angular momentum is explicitly conserved (Benz 1990) and angular momentum losses are limited to round-off errors (roughly one part in a million for our simulations). However, angular momentum can be transported artificially in these simulations. To test whether the transport of angular momentum in Fig. 9 was numerical or real, we ran 2 additional models: a high resolution run (SN15A-hr) where the effects of artificial SPH viscosity should be diminished, and a run where the SPH viscosity is reduced by a factor of 10 (SN15A-rv). If the effects of numerical viscosity were indeed the culprit behind the angular momentum transport, the high-resolution and reduced viscosity simulations should have yielded quite different results from model SN15A. However, as we see from the angular velocity distribution in Fig. 10, there is very little difference between these 3 rotating simulations.

How can we explain the outward movement (in mass zones) of the angular momentum? As the core contracts, the material with greater angular momentum is slowed by centrifugal forces. It does not collapse as deeply as the low angular momentum material and piles up at higher radii where we find much of the angular momentum deposited. Fig. 11 shows the distribution of material in model SN15A 90 ms before bounce which ultimately contracts to form the proto-neutron star. A large fraction of the material below the isocontour boundaries collapses down to 12.5, 20, 50 km 140 ms after bounce. The actual fraction is denoted by solid (65%) and dotted (95%) lines. Figure 10 tells us what part of the original star collapses within 12.5, 20, 50 km and ultimately forms the neutron star. Material in the equator does not contract so quickly and does not initially become part of the neutron star and the neutron star mass is originally biased toward the low angular momentum material of the polar region. This is not to say that the high angular momentum material will not ultimately become part of the neutron star. Much of this material will slowly find its way on to the proto-neutron star as it either cools and loses pressure support or sheds some of its angular momentum along with some mass, losing the support of centrifugal forces.

Note that if we had assumed that the angular momentum was conserved with mass down through collapse, we would have overestimated the angular momentum in the inner core by roughly a factor of 5 (and hence the total rotational energy by over an order of magnitude). With this revised understanding of the angular momentum distribution, let's study the additional rotational effects on the supernova explosion.

4.1. Core Fragmentation

There has been a growing number of recent papers reviving the idea that fragmentation can occur in the collapse of massive stars (Fryer, Woosley, & Heger 2000; Davies et al. 2002; Colpi & Wasserman 2002). However, the conditions to cause fragmentation are extreme, requiring rotation rates that can hang up the infalling material, causing the density to peak, not in the center, but in a torus. Even with these conditions, many simulations find that the torus then forms a bar (not separate fragments) and ejects its angular momentum to coalesce into a single compact object (e.g. Centrella et al. 2001).

Even our fastest rotating cores do not lead to fragmentation of the core. The nature of rotating, gravitationally-bound objects is fairly well determined by the ratio of rotational energy over the magnitude of the gravitational binding energy: $T/|W| = 0.5 I_{\rm core}\Omega_{\rm core}^2/(GM_{\rm core}^2/R_{\rm core})$. Here $I_{\rm core}, \Omega_{\rm core}, M_{\rm core}, R_{\rm core}$ are, respectively, the collapsed core's moment of inertia, angular velocity, mass, and radius and G is the gravitational constant). This ratio as a function of enclosed core mass for our 3 rotating progenitors (SN15A, SN15B, and SN15C) 45 ms after bounce is plotted in Fig. 12. If the density is centrally peaked, this ratio must exceed ~ 0.14 for the core to be secularly unstable. Given that the angular momentum can be transported outward, dynamical instabilities ($T/|W| > 0.25$) are probably required to produce bar instabilities and fragmentation. Note that only our fastest rotating star (SN15B) has values even close to this secular instability. It is therefore unlikely that any of these models will develop bar modes, let alone fragment, at these early times. Not surprisingly, bar modes do *not* develop in any of our simulations and, likewise, fragmentation is not an issue.

Indeed, even if the star is dynamically unsta-

ble, fragmentation is most likely when the density profiles are not centrally peaked. Such toroidal density profiles are more likely to become dynamically unstable (Centrella et al. 2002 and references therein) and could then more easily fragment. Note, however, that the Centrella et al. (2002) simulations did not show fragmentation even though the star was dynamically unstable and toroidal density distributions are probably a necessary, but not sufficient, condition for fragmentation. With our more moderate rotation speeds, we would expect ellipsoidal density configurations such as Maclaurin spheroids. Our simulations did relax into these aspherical density profiles (Fig. 6). With these centrally peaked density profiles, it is extremely unlikely that fragmentation or dynamical bar instabilities will occur with any of the currently-produced supernova progenitors. Despite the recent burst of papers on fragmentation in core-collapse, it is almost certain that fragmentation will only occur in rare collapse cases where the star has been spun up prior to collapse (e.g. in Fryer et al. 2001, the collapsed "core" consisted of the central $\sim 50 M_\odot$ of a collapsing $300 M_\odot$ star, the outer layers of which contained a great deal of angular momentum). If the current collapse progenitors are typical for supernova progenitors, most collapsing stars will not fragment.

4.2. Magnetic Field Driven Explosions

Even with the redistribution of angular momentum, as the core contracts, the rotational energy in the star increases. A number of mechanisms exist in which rapidly rotating proto-neutron stars can generate magnetic fields (e.g. Thompson & Duncan 1993, Akiyama et al. 2003). Whether or not these magnetic fields can play the dominant role in driving the explosion relies upon how quickly such magnetic fields can develop (if an explosion is not launched quickly - within the ~1st second after bounce - the proto-neutron neutron star will accrete too much material and collapse into a black hole). The dynamo proposed by Thompson & Duncan (1993) is unlikely to make a strong magnetic field until the neutron star cools, contracts, and spins up. This dynamo can easily make magnetar fields in the cooling neutron star after the launch of the explosion, but Fryer & Heger (2000) found that this dynamo could not make strong enough fields to effect the convective region in the first second after bounce. It is in this first second that the star either explodes or collapses down to a magnetic field and it is thus unlikely that this dynamo mechanism will produce the initial supernova explosion.

Akiyama et al. (2003) argue that a very effective magnetic field process can arise from the differential rotation in the core. Once these magnetic fields form, they argue that these magnetic fields can extract rotational kinetic energy to drive a supernova explosion. The saturation magnetic field B arising from differential rotation is given by (Akiyama et al. 2003):

$$B^2 \sim 4\pi\rho r^2\Omega^2(d\ln\Omega/d\ln r)^2 \qquad (5)$$

where ρ is the density and Ω the angular velocity at a radius r in the proto-neutron star. Even for our most rapidly rotating progenitors, it is difficult to produce magnetic fields in excess of 10^{14}G (Fig.13). Although the rotational energy in our fastest rotating cores can exceed 10^{51} erg (Tab. 1), the estimated magnetic fields are too weak to effectively use this energy and dominate the explosion. Even so, we can not rule out that magnetic fields can't play some role driving further asymmetries in the ejecta. For our slow rotating (SN15A) progenitor, magnetic field driven effects will not become important until after the proto-neutron star cools and contracts, the total rotational kinetic energy in the proto-neutron star (and in the entire core for that matter) is insufficient to produce a 10^{51} erg explosion.

It appears that magnetic field mechanisms are unlikely engines to dominate the supernova explosion for most supernovae, but we can not rule out that magnetic fields won't play any role on the explosion. Of course, if the explosion were to be launched several seconds after the bounce of the core (when the star has collapsed to a black hole), there would be ample magnetic fields and rotational energy to drive an explosion for our rapidly rotating progenitors (SN15A, SN15B). Such an explosion mechanism is known as a collapsar (Woosley 1993) and has been suggested as a gamma-ray burst and hypernova engine.

4.3. Pulsar Emission and the Supernova Explosion

Another way that magnetic fields can effect the explosion is through intense pulsar emission shortly after the explosion. A millisecond pulsar with a strong magnetic field could easily inject a 10^{51} erg jet into the expanding supernova ejecta. Such a jet would significantly alter the observed supernova spectra, polarization and light curve. Here we discuss the expected spin periods from our simulations and the magnetic fields required to cause the pulsar emission to dominate the supernova light curve.

If we take the total angular momentum in the $1.0\,M_\odot$ proto-neutron star at the end of our simulations and conserve it as it contracts into a 12.5 km neutron star, model SN15B would produce a a sub-millisecond pulsar. However, beware of such calculations. We are estimating the spin period by assuming that the angular momentum will be conserved as the proto-neutron star collapses. For models SN15A and SN15C, where we have late-time calculations, we find that the inner core continues to lose angular momentum. 45 ms after bounce, if we took the inner core of model SN15C and collapsed it, conserving angular momentum, we would find that the neutron star would have a spin of 12 ms. 90 ms later, the collapsing core had only enough angular momentum to produce a 17 ms pulsar. It is likely that the spin period of this slow rotating model will ultimately be greater than 20 ms.

Why does this occur? As we showed in Fig. 8, much of the high angular momentum material does not collapse directly into the proto-neutron star. Its centrifugal support slows its collapse and the high angular momentum material does not immediately become part of the proto-neutron star. As the proto-neutron star contracts further, this high angular momentum will not contract with it but will hang up in a disk around the proto-neutron star. The high angular momentum material may well lose much of its angular momentum before accreting onto the neutron star through transport out the the disk or in a wind. Recall, that it requires nearly 10^{51} ergs of energy to eject $10^{-4}\,M_\odot$ on the surface of a 20 km neutron star. If the wind or disk outflows extract rotation energy, much of the rotational energy may be lost in ejecting only a small amount of material off the disk surface. It is much easier to transport angular momentum outwards than compress high angular momentum material onto the proto-neutron star. Hence, the spin periods listed in Table 1 should be seen as *upper limits*.

Pulsars with the slow rotation periods predicted for our slowly rotating progenitor (SN15C) will not be bright enough to drastically change the supernova explosion energy, no matter what the magnetic field strength. However, our fast rotating progenitors could easily produce 1-2 ms pulsars that, with sufficiently high magnetic fields, could inject energies comparable to the supernova explosion itself. A pulsar born with a 1 ms period and a 10^{12} G magnetic field would inject a 2×10^{50} erg jet during its first year. This is roughly 10-20% of the total supernova energy and may be detectable in the supernova lightcurve. A similar pulsar with with a 10^{13} G magnetic would inject nearly 5×10^{51} erg in a jet. This would dominate the supernova explosion energy. It may be that the peculiar lightcurves and spectra of some supernova are exactly such objects: fast spinning, high magnetic field pulsars.

We discuss pulsar emission and spin rates in more detail in §5.

5. Other Rotational Observables: Pulsars, Gravitational Waves and Nucleosynthesis

In this paper, we have studied the collapse of a number of rotating and non-rotating stars to probe the effects of rotation on supernovae. We found that for our fastest rotating progenitor stars (the fastest pre-collaapse produced by modern stellar evolution models), rotation can indeed produce asymmetries asymmetries in the explosion. However, the cores these stars did not fragment in our collapse simulations and analysis of the rotation suggest that the rotation rate must be much higher than predicted by Heger et al. (2000) to cause the proto-neutron star to fragment. Even if magneto-hydrodynamic instabilities are as efficient as Akiyama et al. (2003) claim, magnetic instabilities will not dominate the explosion. But we can not rule out that they won't play any role in the explosion mechanism. Indeed, if the magnetic field of the resultant pulsar is greater than

$\sim 10^{12}$ G, the pulsar emission will alter the supernova explosion. However, if the star is slowly rotating, as predicted by Heger et al. (2003), rotationally-driven effects will not occur and we can rule out rotation as an important effect in core-collapse supernovae.

The explosion asymmetries from our fastest rotating stars provide an easy explanation for the outward mixing of nickel and anomolous ^{44}Ti yields observed in supernova 1987A (Nagataki 2000, Hungerford et al. 2003). Whether such high rotation velocities occur in stars is a crucial uncertainty in understanding the fate of massive stars. Unfortunately, stellar models are not yet sophisticated enough to say whether nature produces fast (Heger et al. 2000) or slow (Heger et al. 2003) rotating cores, and it is unlikely that stellar evolution models with accurate magnetic field and angular momentum transport algorithms will exist in the near future.

However, there are a number of other indirect methods by which we can determine the rotation of the stellar core before collapse. One is the emission from young pulsars. As we discussed in §4.3, a rapidly spinning, high magnetic field, pulsar can emit enough energy to impact the supernova explosion. There is a large database of observed pulsars which, if we could determine their spin evolution since birth, would give us a clue about the birth spin rates of pulsar. The critical uncertainty here is determining how the spins of pulsars evolve. Figure 14 shows pulsar luminosities as a function of time for a range of pulsar initial conditions and properties. One of the key uncertainties in such a calculation is the role of r-modes to spin down the pulsar. Recent results show that the r-mode amplitude ($\alpha_{\rm r-mode}$) will not exceed 10^{-3} (e.g. Schenk et al. 2002) but this constraint strongly depends upon the neutron star equation of state and the particular r-mode instability (e.g. Lee & Yoshida 2003). To get a flavor of the range of results, we use the pulsar evolution code developed in Fryer, Holz, & Hughes (2002) following the formalism of Ho & Lai (2000). We have run models with r-mode maximum amplitudes ($\alpha_{\rm r-mode}$) of 10^{-3} and 10^{-2} which we assume to *not* be dependent upon the temperature evolution of the neutron star. This overestimates the strength of the true r-mode instability. Below a maximum amplitude of 10^{-3}, r-modes play very little role in the pulsar luminosity. By 1000 years, even amplitudes as high as 10^{-2} does not alter the pulsar luminosity significantly. Likewise, a star initially rotating at 10 ms will appear very similar to a a 1 ms initial rotating pulsar within 10,000 years after the supernova explosion. It would be difficult to distinguish 200 years after the supernova explosion a 1 ms pulsar whose magnetic field decays from 10^{13}G down to 10^{12}G after 200 years from a 10 ms whose magnetic field remained constant at 10^{12}G for those 200 years.

These similarities are due to the fact that pulsars lose most of their angular momentum early in their evolution. It takes less than 100 years for a 1 ms pulsar to spin down to a 2 ms pulsar (Fig. 15). A 10^{13} G, 1 ms pulsar will have a period longer than 1 s after 1 million years.

Very few pulsars have age determinations that are independent of the spin-down rate, so it is very hard to determine the true birth spin of pulsars. Estimates of the birth spin rates range from 2 ms (Middleditch et al. 2000) to well above 100 ms (Romani & Ng 2003). However, all these estimates suffer from many uncertainties and it is difficult to constrain stellar rotation rates from observations of pulsar spins. In general it is believed that some pulsars were probably born with spin periods faster than 10 ms, but some are also born with much slower spin periods. If some pulsars are born with spin periods faster than 10 ms, some stellar cores must be rotating faster than our slowly rotating progenitor (SN15C). If all pulsars are born with spin rates above 20 ms, our fast rotating models will have to lose considerable angular momentum as they contract. But there are models to spin up neutron stars and mechanisms to remove angular momentum, so it is unclear if pulsar observations can rule out any progenitor.

A more promising constraint on the initial rotating periods of massive stars is the gravitational wave signal. In Fig. 16, we plot the gravitational wave signal (amplitudes) for model SN15B-nr and SN15B. The signal from the rotating progenitor can be over a factor of 5 higher than the non-rotating case. Even so, the signal is not strong enough to be observable by advanced LIGO (see Gustafson et al. 1999 or Fryer, Holz, & Hughes 2002). But a galactic supernova would easily have a strong enough signal to distinguish our fast rotating models (SN15A,SN15B) with our slow ro-

tating progenitor (SN15C) or non-rotating progenitors. Indeed, it is likely that a galactic supernova will provide enough of a signal to distinguish rotating models from other asymmetries in the core-collapse (see Fryer, Holz, Hughes 2003 for more details).

Nuclear yields from supernova explosions could also place constraints on the rotation. The temperatures in the rotating core are roughly symmetric (Fig. 17), slightly peaking in the polar region. However, high density contours extend much further out in the equator (Fig. 6), so the neutrinosphere is deeper in along the poles than along the equator. These two effects both cause neutrinos arising from the polar region to have higher mean energies than those in the equator. The neutrino-driven wind will be far from symmetric, and the r-process yields may differ considerably from that predicted by symmetric wind calculations.

We are grateful A. Heger for useful discussions and support. This work was funded under the auspices of the U.S. Dept. of Energy, and supported by its contract W-7405-ENG-36 to Los Alamos National Laboratory and by a DOE SciDAC grant number DE-FC02-01ER41176. The simulations were conducted both on the ASCI Q machine and the Space Simulator, both at Los Alamos National Laboratory.

REFERENCES

Akiyama, S., Wheeler, J. C., Meier, D. L., & Lichtenstadt, I. 2003, ApJ, 584, 954

Bazan, G., & Arnett, D. 1998, ApJ, 496, 316

Benz, W. 1990, in The Numerical Modeling of Nonlinear Stellar Pulsations, ed. J. R. Buchler, 269

Burrows, A., Hayes, J., & Fryxell, B. A. 1995, ApJ, 450, 830

Colpi, M., & Wasserman, I. 2002, ApJ, 581, 1271

Davies, M.B., King, A., Rosswog, S., & Wynn, G. 2002, ApJ, 579, L63

Dimmelmeier, H., Font, J. A., & Müller, E. 2002, A&A, 393, 523

Endal, A. S., Sofia, s. 1978, ApJ, 220, 279

Fryer, C. L. 1999, ApJ, 522, 413

Fryer, C. L. & Heger, A. 2000, ApJ, 541, 1033 - FH

Fryer, C. L., Woosley, S. E., & Heger, A. 2001, ApJ, 550, 372

Fryer, C. L., Holz, D. E., & Hughes, S. A. 2002, ApJ, 565, 430

Fryer, C. L. & Warren, M. S. 2002, ApJ, 574, L65

Fryer, C. L., Holz, D. E., & Hughes, S. A. 2003, in preparation

Gustafson, E., Shoemaker, D., Strain, K., Weiss, R. 1999 LSC White Paper on Detector Research and Development, LIGO Document T990080-00-D.

Heger, A., Langer, N., & Woosley, S. E. 2000, ApJ, 528, 368

Heger, A., Woosley, S. E., & Spruit, H. 2003, in preparation

Herant, M., Benz, W., Hix, W.R., Fryer, C.L. & Colgate, S.A. 1994, ApJ, 435, 339

Ho, W. C. G., & Lai, D. 2000, ApJ, 543, 386

Höflich, P., Wheeler, J. C., Hines, D. C., & Trammell, S. R. 1996, SpJ, 459, 307

Hungerford, A. L., Fryer, C. L., & Warren, M. S. 2003, accepted by ApJ

Iwamoto, K. et al. 1998, Nature, 395, 672

Janka, H.-Th., & Müller, E. 1996, A&A, 306, 167

Kotake, K., Yamada, S., & Sato, K. 2003, accepted by ApJ

LeBlanc, J. M. & Wilson, J. R. 1970, ApJ, 161, 541

Lee, U., & Yoshida, S. 2003, ApJ, 586, L403

Middleditch, J. et al. 2000, New Astronomy, 5 243

Müller, E. & Hillebrandt, W. 1981, A&A, 103, 358

Nagataki, S. 2000, ApJS, 127, 141

Centrella, J. M., New, K. C. B., Lowe, L. L., & Brown, J. D. 2001, ApJ, 550, L193

New, K. C. B. 2003, Living Riviews in Relativity, 6, 2

Rampp, M., & Janka, H.-T. 2002, A&A, 396, 361

Romani, R. W., & Ng, C.-Y. 2003, ApJ, 585, L41

Schenk, A. K., Arras, P., Flanagan, É. É., Teukolsky, S. A., and Wasserman, I. 2002, PRD, 65, 4001

Shimizu, T., Yamada, S., & Sato, K. 1994, ApJ, 432, L119

Wang et al. 2002, ApJ, 579, 671

Warren, M.S., & Salmon, J.K. 1993, In Supercomputing '93, 12-21, 1993 IEEE Comp. Soc.

Warren, M.S., & Salmon, J.K. 1995, Computer Physics Communications, 87, 266

Warren, M.S., Rockefeller, G., & Fryer, C.L. 2003, in preparation

Woosley, S. E. 1993, ApJ, 405, 273

This 2-column preprint was prepared with the AAS LaTeX macros v5.0.

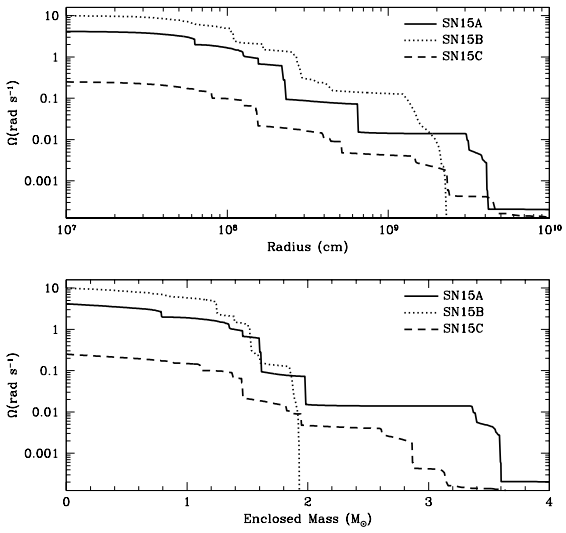

Fig. 1.— Angular velocity versus radius (top) and mass (bottom) for our 3 basic progenitors: SN15A, SN15B, (models E15A and E15B from Heger, Langer, & Woosley 2000) and SN15C ($15\,M_\odot$model from Heger, Woosley, & Spruit 2003). The angular velocity remains relatively constant in burning shells due to convection which efficiently transports angular momentum. However, at the boundaries of these layers, the spins can decouple, causing jumps in the angular velocity. These jumps persist, although with much smaller magnitudes, in the progenitor (SN15C) which includes magnetic fields (which can transport angular momentum across these boundaries). Note that FH erroneously plotted model SN15A instead of the model they used for their simulations (SN15B) in their Fig. 3.

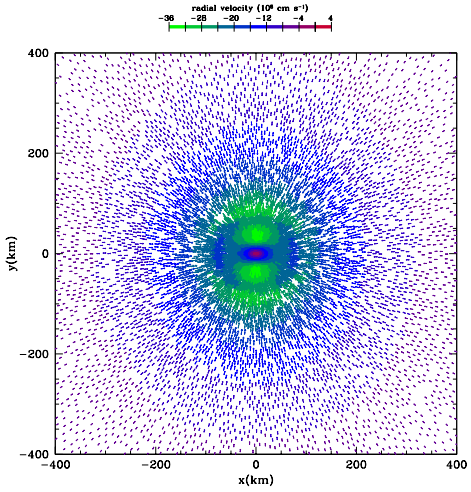

Fig. 2.— An angular slice (0.5°) in the x-z plane of model SN15A-hr just before bounce. By angular slice of 0.5°, we mean: $|y|/\sqrt{x^2+y^2+z^2} < \sin 0.5°$. The colors denote radial velocity and the vectors denote velocity direction and magnitude (vector length). The material in the equator (x-axis) is slowed by centrifugal forces and hence has a slower infall velocity than the material in the poles.

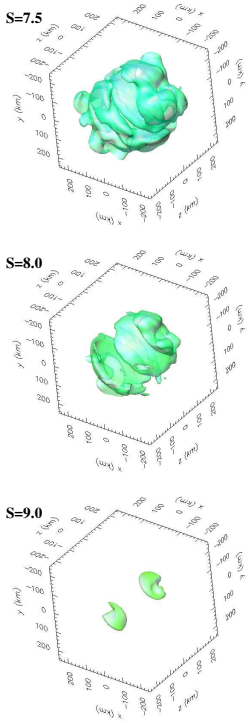

Fig. 3.— Entropy isosurfaces (entropies of $7.5, 8.0, 9.0 k_B$ per nucleon) for model SN15A-hr 45 ms after bounce. Because the velocities are much higher along the poles (Fig. 2), the shock is stronger, producing higher entropy material in this region after bounce. Hence, the highest entropy material is limited to the polar caps.

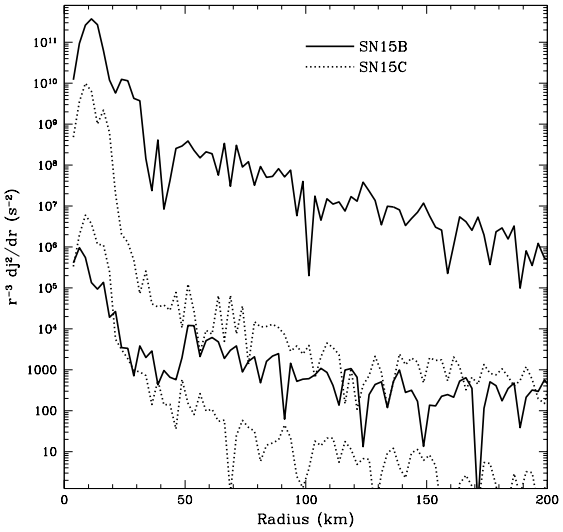

Fig. 4.— The effect of angular momentum on convective instabilities (second term in equation 3) for our fastest rotating model (SN15B - solid lines) and our slowest rotating model (SN15C - dotted lines). The upper curve is this term along the equator, the lower curve is this term along the rotation axis. Not surprisingly, this value is low along the rotation axis. Note also, that in the convection region, (beyond 50 km), the value is 4 orders of magnitude lower in the slowly rotating model (SN15C) than in the fast rotating model (SN15B). It is thus not surprising that rotation plays a much stronger role in the convection for model SN15B than in SN15C. Indeed, in figure 5, we see that the convection in the slow rotating model compares better with the non-rotating cases than our fast rotating models (SN15A and SN15B).

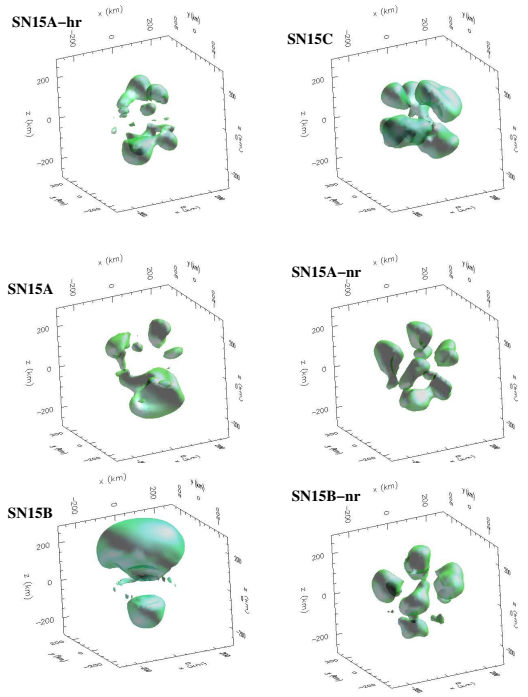

Fig. 5.— Upward moving material (isosurfaces of material moving with outward radial velocities of 3000 km s^{-1}) for many of our models 45 ms after bounce. Note that the fast rotating models (SN15A, SN15A-hr, and SN15B) all convect most strongly along the poles, whereas the convection in the non-rotating or slowly rotating models (SN15A-nr, SN15B-nr, and SN15C) have no preferred direction.

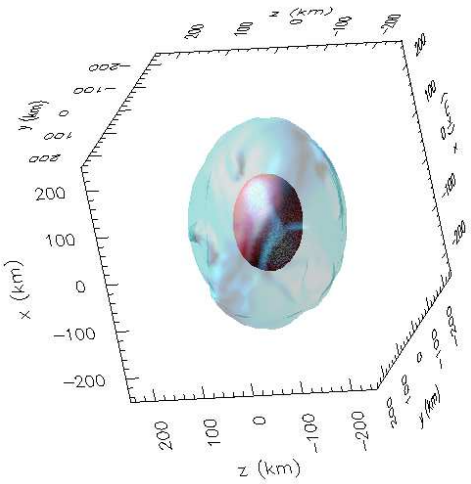

Fig. 6.— Density isosurfaces (10^{11} (blue), 10^{12} (red) g cm^{-3}) of model SN15B-hr 45 ms after bounce. Note that the density structure is asymmetric even at the compact structure of the high density (10^{12}g cm^{-3}) isosurface. Although the structure is asymmetric, the density remains centrally peaked (not toroidal), making it less easy to develop bar instabilities or fragment.

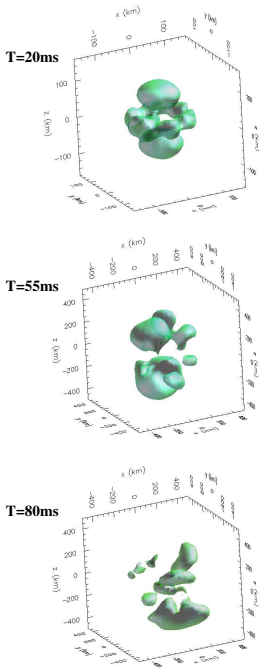

Fig. 7.— Upward moving material (isosurfaces of material moving with outward radial velocities of $1000\,\mathrm{km}\,s^{-1}$) for model SN15A 20, 55, and 80 ms after bounce. The bulk of the upflows are constrained along the rotation axis, in agreement with the 2-dimensional results of FH. Ultimately, this convection will drive a stronger explosion along the poles.

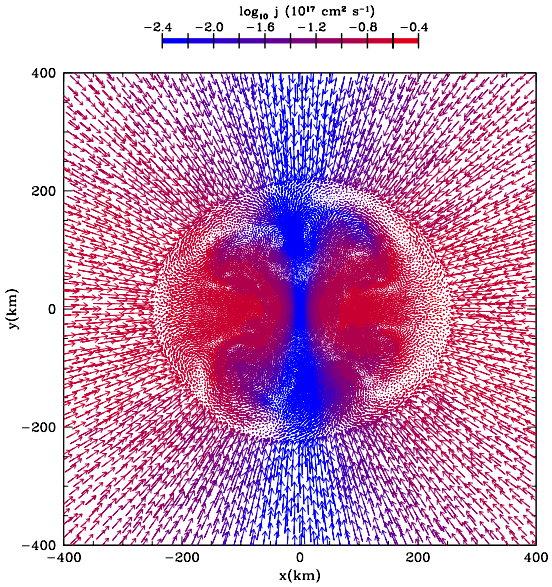

Fig. 8.— An 0.5° angular slice (see Fig. 2 for details) 40 ms after bounce of SN15A-hr. The colors denote the specific angular momentum of the material and the vectors show velocity direction and magnitude (vector length). Note that the bulk of the angular momentum lies along the equator (the angular momentum in the a 15° cone along the poles is 2 orders of magnitude less than that in the equator). The specific angular momentum in the equator is over $10^{16}\mathrm{cm}^2\mathrm{s}^{-1}$, corresponding to a rotation velocity of nearly $5000\mathrm{kms}^{-1}$ and a rotational period of 250 ms.

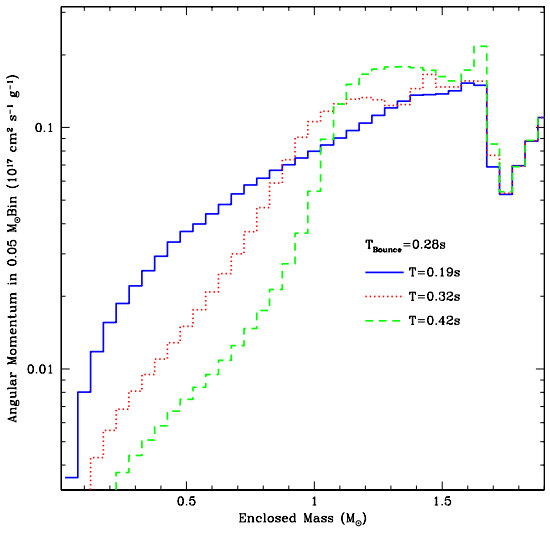

Fig. 9.— Angular momentum versus mass zone as a function of time. The solid line shows the angular momentum profile 90 ms before bounce, the dotted line is 40 ms after bounce, and the dashed line is 140 ms after bounce. Note that in the proto-neutron star interior, the star quickly loses 80% of its total angular momentum. This angular momentum is transported to the surface of the proto-neutron star (note the rise in angular momentum beyond 1 $M_\odot$ 140 ms after bounce).

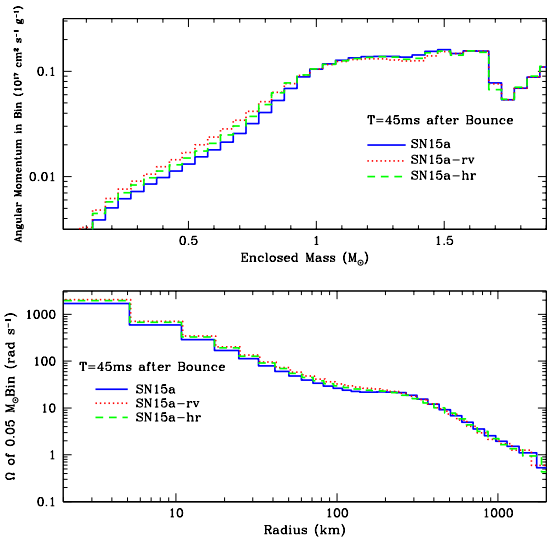

Fig. 10.— Angular momentum versus mass (top) and radius (bottom) for 3 separate models (SN15a: solid line, SN15a-rv: dotted line, SN15-hr: dashed line). From Fig. 8, we note that by 45 ms after bounce, considerable transport has already occured. However, the differences between the high resolution (SN15A-hr), reduced viscosity (SN15A-rv), and standard (SN15A) models are small. If the angular momentum transport were numerical, one would expect the high resolution and reduced viscosity runs would have different results. Although slightly less transport has occured in the reduced viscosity run, there is not a factor of 10 difference which one would expect by decreasing the viscosity by a factor of 10. We can be reasonably assured that the transport is not a numerical artifact.

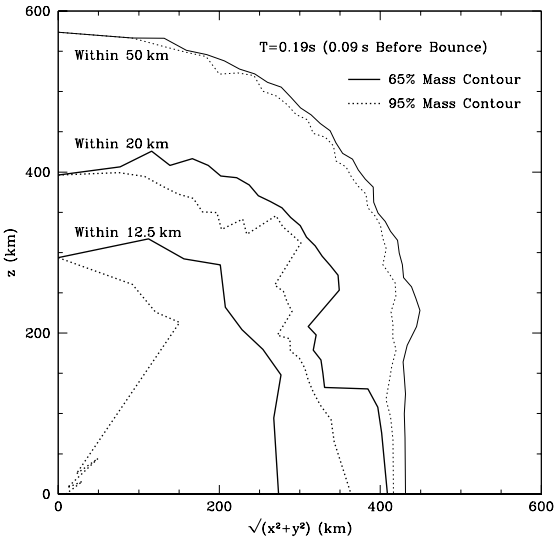

Fig. 11.— Distribution of material in model SN15A 90 ms before bounce which ultimately contracts to form the proto-neutron star. A large fraction of the material below the isocontour boundaries collapse down to 12.5, 20, 50 km 140 ms after bounce. The fraction of material at these boundaries which actually collapses down to 12.5, 20, or 50 km 140 ms after bounce is denoted by solid (65%) and dotted (95%) lines. This figure shows us what part of the original star collapses within 12.5, 20, 50 km and ultimately forms the neutron star. Material in the equator does not contract so quickly and does not initially become part of the neutron star and the neutron star mass is originally biased toward the low angular momentum material of the polar region.

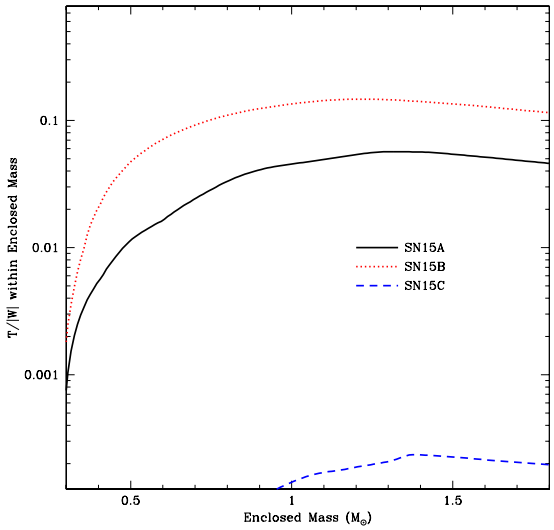

Fig. 12.— The summation of the ratio of kinetic energy over potential energy $T/|W|$ versus enclosed mass for our 3 rotating models: SN15A (solid), SN15B (dotted), and SN15C (dashed). For centrally peaked density profiles of our collapse models, this ratio must be above ~ 0.25 to produce dynamical instabilities. For secular instabilities, this critical value is only ~ 0.14 and model SN15B slightly exceeds this value (it peaks at 0.147), but it is unlikely that secular instabilities will lead to fragmentation. It is highly improbable that fragmentation will occur for most core-collapse supernovae. Indeed, from this figure we see that it is unlikely that core-collapse stars will have any bar instabilities.

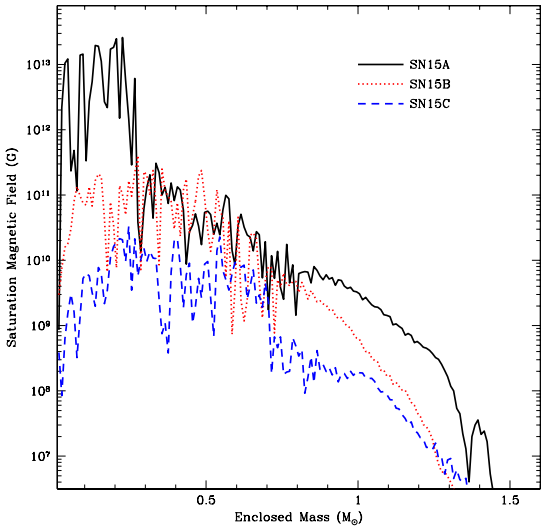

Fig. 13.— Saturation magnetic field strength vs. enclosed mass for our 3 rotating progenitors (SN15A, SN15B, SN15C). Note that the magnetic fields are much smaller than that predicted by Akiyama et al. (2003) and never exceed 10^{14}G. Such weak magnetic fields will not dominate the explosion mechanism, but may alter the convection enough to drive asymmetries. However, the strength of the magnetic field will depend strongly on how compressed the proto-neutron star can become. At later times, or with a different equation of state for nuclear matter, magnetic fields may become more important.

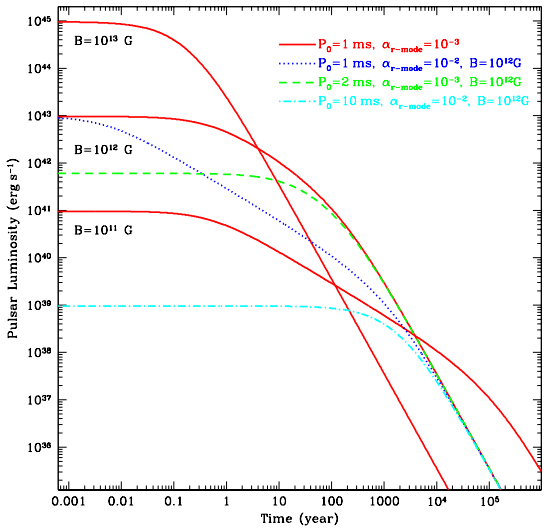

Fig. 14.— Pulsar luminosity vs. time since formation. The solid lines denote pulsars with initial spin periods of 1 ms, maximum r-mode amplitudes: $\alpha_{\rm r-mode} = 10^{-3}$, and a range of magnetic field strengths ($10^{11}, 10^{12}, 10^{13}$ G). The dotted,dashed lines show the evolution of a 10^{12} G field neutron star with, respectively, a higher maximum r-mode amplitude: $\alpha_{\rm r-mode} = 10^{-2}$ and a 2 ms initial period. Note that after 1000 years, it is very hard to distinguish different the initial structure of the star by its luminosity.

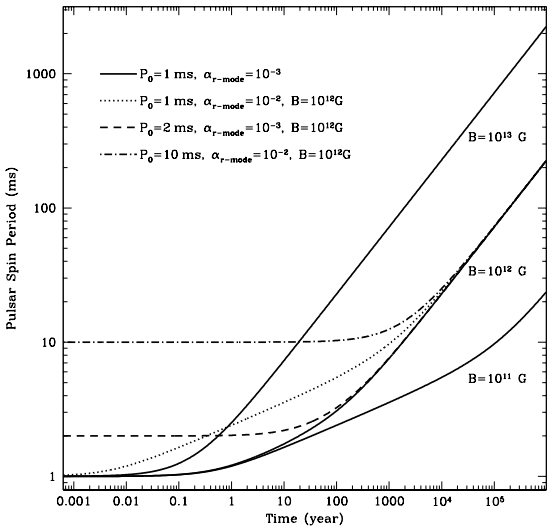

Fig. 15.— Pulsar spin vs. time since formation. The solid lines denote pulsars with initial spin periods of 1 ms, maximum r-mode amplitudes: $\alpha_{\rm r-mode} = 10^{-3}$, and a range of magnetic field strengths $(10^{11}, 10^{12}, 10^{13}\,{\rm G})$. The dotted,dashed lines show the evolution of a 10^{12} G field neutron star with, respectively, a higher maximum r-mode amplitude: $\alpha_{\rm r-mode} = 10^{-2}$ and a 2 ms initial period. Note that after 1000 years, it is very hard to distinguish different the initial structure of the star by its spin.

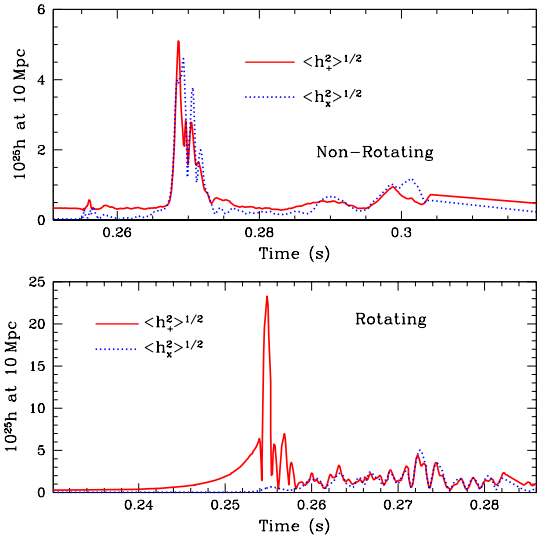

Fig. 16.— The angle averaged wave amplitudes ($< h_+^2 >^{1/2}$: solid line,$< h_x^2 >^{1/2}$: dotted line) for models SN15B-nr (top) and SN15B (bottom) versus time. Note that the gravitational wave signal is a factor of 5 higher for the rotating model. A galactic rotating supernova would be detectable by advanced LIGO.

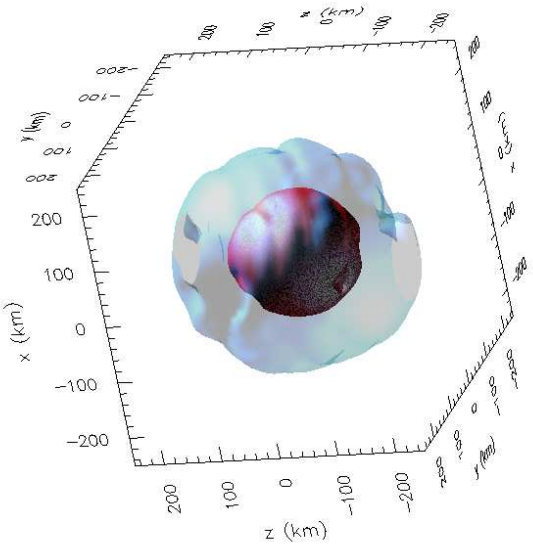

Fig. 17.— Temperature isosurfaces (2×10^{10} (blue), 3.5×10^{10} (red) K) of model SN15B-hr 45 ms after bounce. Note that the temperatures are only slightly asymmetric (with peaks in the polar regions). The lower optical depth in the polar regions (see density profiles in Fig. 6) along with the higher temperatures in the poles lead to a hotter neutrino flux along the poles, and hence a higher entropy outflow.

TABLE 1

CORE-COLLAPSE SIMULATIONS

Model	Resolution (No. of Particles)	$P_{\rm core}^{\rm beforecollapse}$ [a] (s)	$\rho_{\rm bounce}$ [b] (10^{14} g cm^{-3})	$E_{\rm rot}^{45\,\rm ms}$ [c] (10^{51} ergs)	$T/\lvert W\rvert^{45\,\rm ms}$ [d]	$B_{\rm max}^{45\,\rm ms}$ [e] (G)	$P_{\rm NS}$ [f] (ms)
SN15A	1 million	1.5	2.8	5(2)	0.056 (0.035)	10^{13}	0.65 (0.91)
SN15A-hr	5 million	1.5	2.3	4	0.052	10^{13}	0.66
SN15A-rv	1 million	1.5	2.8	6	0.062	10^{13}	0.64
SN15A-nr	1 million	0	3.5	< 0.001	$< 10^{-4}$	$< 10^{9}$	> 1000
SN15B	0.5 million	0.63	2.0	7	0.156	10^{11}	0.35
SN15B-nr	1 million	0	3.5	< 0.001	$< 10^{-4}$	$< 10^{9}$	> 1000
SN15C	1 million	25	3.4	0.02 (0.02)	2.3×10^{-4} (2.0×10^{-4})	$< 10^{10}$	12 (17)

[a] Rotation Period of the inner core from Heger et al. (2002,2003) at collapse.

[b] Density when the core "bounces" and drives a shock out through the star.

[c] Rotational energy of the inner 1.2 $M_\odot$, 45 ms after bounce. We have also included, in parantheses, the rotational energy for models SN15A 160 ms after bounce and SN15C 135 ms after bounce.

[d] The maximum of the ratio of kinetic to the absolute value of the gravitational potential energy 45 ms after bounce. This value should be above ~ 0.14 to have any chance of driving significant bar instabilities. As with the rotation energy, the paranthetical values are for models SN15A 160 ms after bounce and SN15C 135 ms after bounce.

[e] Saturation magnetic field strengths using equation 5 45 ms after bounce.

[f] Pulsar spin periods assuming that the angular momentum in the inner 1.0 $M_\odot$ is conserved as the star collapses down to to a neutron star. The paranthetical values are for models SN15A 160 ms after bounce and SN15C 135 ms after bounce. Note that the inner core continues to lose angular momentum. Model SN15C is unlikely to produce pulsars with spin periods faster than 20 ms. and it is unlikely that sub-millisecond pulsar will form from any model.